

Toroidal orders and related phenomena in nonmagnetic and magnetic materials

Hiroaki Kusunose^{1,2} & Satoru Hayami³

¹Department of Physics, Meiji University, Kawasaki 214-8571, Japan

²Quantum Research Center for Chirality, Institute for Molecular Science, Okazaki 444-8585, Japan

³Department of Applied Physics, the University of Tokyo, Tokyo 113-8656, Japan

E-mail: hk@meiji.ac.jp

Abstract. In this short article, we overview a concept of electronic toroidal multipoles, and their ordering with associated physical properties in non-magnetic and magnetic materials. The toroidal multipoles are introduced as microscopic electronic variables in view of symmetry and connection to Dirac theory. They are classified according to crystallographic and magnetic point groups, which allows us to discuss various possible cross correlations in a transparent and unified manner. The representative examples of toroidal orders and related phenomena, and the mutual relationship between these orders are given, with focusing on monopoles and dipoles. The concept of toroidal multipoles would promote future studies toward observations and identifications of unknown electronic phases and their related physical phenomena.

1. Introduction

Symmetry of materials and their physical properties are closely related. Representative examples that spontaneously break fundamental symmetries, i.e., the time-reversal and spatial inversion symmetries, are ferromagnetism and ferroelectricity, respectively. They are long-range order of microscopic variables, magnetic (M) and electric (E) dipoles. In recent years, it has been extensively investigated alternative orders that break both time-reversal and spatial inversion symmetries [1, 2, 3] or do not break both of them [4, 5]. They are called as toroidal or ferroaxial orders, respectively. These orders are characterized by the alignment of a certain type of microscopic variables as well, which are the main subject of the present paper.

In contrast to an electron in vacuum, electrons in materials have a rich variety of degrees of freedom, i.e., charge, orbital, spin, and sublattice in underlying molecular or crystal structures. By considering their combinations, various microscopic variables other than ordinary electric and magnetic dipoles can be constructed, which become order parameters of unconventional orders and bring about associated exotic physical properties.

In the classification of electronic degrees of freedom in materials, it has been recognized two types of multipoles, E and M multipoles [6, 7, 8]. Subsequently, additional two types of multipoles, the electric toroidal (ET) and magnetic toroidal (MT) multipoles, that are indispensable for a unified description of a state of matter, have been incorporated [9, 10, 11, 12, 13, 14, 15]. The ET and MT multipoles have the opposite spatial-inversion parity to the conventional E and M multipoles, and these four types of multipoles (E, M, ET, and MT) constitute a complete basis set to describe arbitrary electronic degrees of freedom in materials

Table 1. Symmetry properties of the four types of monopoles and dipoles. \mathcal{M}_\perp (\mathcal{M}_\parallel) represents the mirror operation with respect to the plane perpendicular (parallel) to dipole. $\bar{\mathbf{r}} = \mathbf{r}/|\mathbf{r}|$, \mathbf{l} , and $\boldsymbol{\sigma}$ represent dimensionless position vector, orbital angular momentum, and Pauli matrix, respectively. The definitions of operators, \mathbf{Q}' , \mathbf{G}' , and \mathbf{T}' , are given in [13].

MP	\mathcal{R}	\mathcal{T}	\mathcal{P}	\mathcal{M}_\perp	\mathcal{M}_\parallel	#PG	#MPG	Form (orbital)	Form (spin)	
Q_0	$l=0$	+	+	+	+	32	122	1	$\frac{1}{\sqrt{3}}(\mathbf{l} \cdot \boldsymbol{\sigma})$	
M_0	$l=0$	-	-	-	-		32	—	$\frac{1}{\sqrt{3}}(\bar{\mathbf{r}} \cdot \boldsymbol{\sigma})$	
G_0	$l=0$	+	-	-	-	11	32	—	$\frac{1}{\sqrt{3}}(\mathbf{t} \cdot \boldsymbol{\sigma})$	
T_0	$l=0$	-	+	+	+		32	i (off-diagonal)	—	
\mathbf{Q}	$l=1$	+	-	-	+	10	31	$\bar{\mathbf{r}}$	$\frac{1}{\sqrt{3}}(\boldsymbol{\sigma} \times \mathbf{t})$	\mathbf{Q}'
\mathbf{M}	$l=1$	-	+	+	-		31	\mathbf{l}	$\boldsymbol{\sigma}$	$\frac{1}{\sqrt{10}}[3(\bar{\mathbf{r}} \cdot \boldsymbol{\sigma})\bar{\mathbf{r}} - \bar{\mathbf{r}}^2 \boldsymbol{\sigma}]$
\mathbf{G}	$l=1$	+	+	+	-	13	43	—	$\frac{1}{\sqrt{2}}(\boldsymbol{\sigma} \times \mathbf{l})$	\mathbf{G}'
\mathbf{T}	$l=1$	-	-	-	+		31	$\mathbf{t} \equiv \frac{1}{6}(\bar{\mathbf{r}} \times \mathbf{l}) + \text{h.c.}$	$\frac{1}{\sqrt{2}}(\boldsymbol{\sigma} \times \bar{\mathbf{r}})$	\mathbf{T}'

in molecules and crystals [16]. For example, ET and MT dipoles are the microscopic variables of ferroaxial and toroidal orders, respectively [2, 3, 17]. On the other hand, the ET monopole having time-reversal even pseudoscalar property is a practical entity of chirality [12, 13, 18, 19], which was thoughtfully discussed by Barron [20, 21, 22]. Moreover, the MT monopole can be realized in certain types of antiferromagnet (AFM) [23], which will be discussed in this paper.

This paper is organized as follows. In Sec. 2, we introduce the concept of toroidal multipole from symmetry viewpoint at the classical and quantum-mechanical level. In addition to this, we show the connection to the chirality in the Dirac theory. Then, we discuss the toroidal orders and related phenomena, with focusing on monopoles and dipoles in Sec. 3. The relation between point groups and active multipoles, and possible cross correlations under multipole orders are also clarified. In Sec. 4, we give prime examples for ET and MT monopole and dipole orders and related phenomena. The final section summarizes the paper.

2. Concept of toroidal multipole

2.1. Multipole and symmetry

It is well known that a charge distribution brings about a polar quantity such as an electric dipole \mathbf{Q} , while an electric current distribution yields an axial quantity such as a magnetic dipole \mathbf{M} . Once such dipoles exist, a vortex-like alignment of them gives us another independent quantity characterized by a dipole ($\mathbf{G} \propto \sum_j \mathbf{R}_j \times \mathbf{Q}_j$ or $\mathbf{T} \propto \sum_j \mathbf{R}_j \times \mathbf{M}_j$ where \mathbf{R}_j is a position of the dipole), which has an opposite spatial parity of \mathbf{Q} or \mathbf{M} as the cross product contains the totally anti-symmetric (Levi-Civita) tensor. This is the so-called electric-toroidal (ET) or magnetic-toroidal (MT) dipole, representing the degree of vorticity of a distribution of electric or magnetic dipoles. The concept of toroidal dipoles (rank $l = 1$ with the component m) can be generalized straightforwardly to any ranks (called a toroidal multipole G_{lm} or T_{lm}) introduced as a classical quantity in the middle of 1980s [9, 10].

The concept of multipole is closely related to the symmetry. The principal symmetry of interest for materials science consists of the time-reversal \mathcal{T} , spatial inversion \mathcal{P} , and rotation \mathcal{R} , while the translational operation is less important in the present argument. As similar to the multipole expansion for characterizing an anisotropic distribution of electromagnetic fields, an anisotropic state of materials can be characterized by “multipoles” with a set of properties of $(\mathcal{T}, \mathcal{P}, \mathcal{R})$, i.e., “electric(+)/magnetic(-)” of \mathcal{T} , “polar $[(-1)^l]$ /axial $[(-1)^{l+1}]$ ” of \mathcal{P} , and (l, m) of \mathcal{R} . The enumeration of all combinations corresponds either to Q_{lm} (electric polar), M_{lm}

(magnetic axial), G_{lm} (electric axial), or T_{lm} (magnetic polar), and hence, these four-type of multipoles constitute a symmetry-adapted complete basis set [11, 12, 13, 14, 15, 16]. In other words, a state of materials is described by a linear combination of these four-type multipole bases as a building block with an emphasis on the symmetry. For instance, the properties of the multipoles for $l = 0, 1$ are summarized in Table 1. It is noted that the mirror operation $\mathcal{M}(\mathbf{n})$ with respect to a plane perpendicular to a unit vector \mathbf{n} is equivalent to \mathcal{P} in addition to 180° rotation around \mathbf{n} [$C_2(\mathbf{n})$], i.e., $\mathcal{M}(\mathbf{n}) = \mathcal{P}C_2(\mathbf{n})$. Therefore, \mathcal{P} and $\mathcal{M}(\mathbf{n})$ have no differences for monopole, while \mathcal{P} and $\mathcal{M}(\mathbf{n})$ for dipole with \mathbf{n} being perpendicular to it (\mathcal{M}_\parallel) differ since $C_2(\mathbf{n})$ gives an additional sign for dipole.

2.2. Symmetry lowering and emergence of multipole

As long as a system is invariant under $(\mathcal{T}, \mathcal{P}, \mathcal{R})$ operations, an electric monopole [$l = m = 0$, $\mathcal{T} = +$, $(\mathcal{P}, \mathcal{M}_\perp, \mathcal{M}_\parallel) = (+, +, +)$], i.e., electric charge, is only allowed to exist. However, since some of $(\mathcal{T}, \mathcal{P}, \mathcal{R})$ is lost in realistic materials, the corresponding multipoles other than Q_0 can appear. In other words, the appearance of multipoles characterizes how the symmetry of a system is lost. In the case of macroscopic systems, such symmetry-adapted multipole represents a possible candidate of order parameter, while for an isolated molecule, it characterizes its wave function in terms of symmetry. Note that \mathcal{P} or $\mathcal{M}(\mathbf{n})$ alone can exist in the case without $C_2(\mathbf{n})$ in some point groups, in contrast to the rotation group where $C_2(\mathbf{n})$ and hence both \mathcal{P} and $\mathcal{M}(\mathbf{n})$ always exist.

As shown above, the toroidal multipole was introduced as a classical quantity, where the dipole moment, \mathbf{Q}_j in \mathbf{G} or \mathbf{M}_j in \mathbf{T} , is the expectation value of the corresponding quantum-mechanical electric or magnetic dipole operator. Therefore, a certain type of antiferromagnets accompany the ferroic ordering of \mathbf{T} which breaks $(\mathcal{T}, \mathcal{P}, \mathcal{M}_\perp)$. Such antiferromagnets have been investigated extensively, referred to as various terms such as magneto-electric, (magnetic) toroidal, anapole, or MT-dipole ordering. Precisely speaking, an MT state is characterized by a component of \mathbf{T} belonging to the identity representation in the ordered phase. UNi_4B [24, 25, 26, 27], $\alpha\text{-Cu}_2\text{V}_2\text{O}_7$ [28, 29, 30, 31], and CuMnAs [32, 33, 34] are the prime examples showing the MT-dipole ordering.

Meanwhile, since the MT monopole T_0 has properties $(\mathcal{P}, \mathcal{M}_\perp, \mathcal{M}_\parallel) = (+, +, +)$ and $\mathcal{T} = -$, an emergence of T_0 breaks only \mathcal{T} symmetry, which mixes between time-reversal partners, i.e., Q_{lm} and T_{lm} or G_{lm} and M_{lm} without changing other symmetry properties. This time-reversal switching aspect due to T_0 leads to intriguing cross correlations as shown later [23]. From a symmetry point of view, T_0 is expressed as $T_0 \propto \sum_j \mathbf{R}_j \cdot \mathbf{T}_j$ for example, which indicates that a vortex-like magnetic structure has a divergent property. The practical examples will be discussed later.

Similarly, a vortex-like alignment of electric dipole moments accompanies a ferroic ordering of \mathbf{G} . Since it corresponds to a static structural rotational distortion, it is called as rotational, ferroaxial, or ET-dipole ordering. The gyrotropic vector, which plays a significant role in optical phenomena in anisotropic media, belongs to the same category of \mathbf{G} from the symmetry of view. In this case, a component of \mathbf{G} becomes the identity representation in the symmetry-lowering state, which breaks the vertical mirror \mathcal{M}_\parallel with keeping \mathcal{T} , \mathcal{P} , and \mathcal{M}_\perp as \mathbf{G} has the properties $(\mathcal{T}, \mathcal{P}, \mathcal{M}_\perp) = (+, +, +)$ and $\mathcal{M}_\parallel = -$. $\text{RbFe}(\text{MoO}_4)_2$ [4, 35], NiTiO_3 [5, 35, 36], and $\text{Ca}_5\text{Ir}_3\text{O}_{12}$ [37, 38, 39, 40, 41] are the prime examples showing the ET-dipole ordering.

Moreover, chirality is characterized by pure rotation operations only with keeping the time-reversal symmetry, and there are no mirror and spatial inversion operations [21, 22, 42, 43]. This type of symmetry breaking corresponds to the emergence of G_0 which has the properties $\mathcal{T} = +$ and $(\mathcal{P}, \mathcal{M}_\perp, \mathcal{M}_\parallel) = (-, -, -)$ [12, 13, 18, 19]. As G_0 is \mathcal{T} -even axial monopole (pseudoscalar), one possible realization of chirality is characterized by $G_0 \propto \sum_j \mathbf{R}_j \cdot \mathbf{G}_j$ for example, which implies a three-dimensional structure containing a divergent character of a vortex-like alignment

of electric dipole moments corresponding to structural chirality.

As shown in the above arguments, a toroidal monopole represents a degree of divergence of corresponding dipole distribution, while a toroidal dipole represents a degree of vorticity (rotation) of opposite-parity dipole distribution. They are comprehensive information of dipole distribution of materials.

2.3. Quantum-mechanical operator for toroidal multipole

In contrast to the above classical view of toroidal multipoles, the quantum-mechanical operators of them in atomic scale were found recently [11, 13]. The expressions of monopoles and dipoles with or without the spin degrees of freedom are summarized in Table 1, and the complete expressions of the atomic-scale multipoles are found in literature [11, 13, 16].

The operator expression for G_0 naturally arises from the Dirac equation [44, 45, 46]. It is well known that for a given four-component wave function $\psi_\mu(x)$, the chiral density $\chi(x)$ at the space-time point $x = (\mathbf{r}, t)$ is expressed as $\chi(x) = \sum_{\mu\nu} \psi_\mu^\dagger(x) \gamma_5^{\mu\nu} \psi_\nu(x)$, where $\gamma_5 = i\gamma^0\gamma^1\gamma^2\gamma^3$ in terms of the Dirac γ -matrices represents the operator of chirality acting on $\psi_\mu(x)$. Note that there is the helicity operator, $\boldsymbol{\Sigma} \cdot \mathbf{p} = -\gamma^0\gamma_5\boldsymbol{\gamma} \cdot \mathbf{p}$ ($\boldsymbol{\Sigma}$ is 4×4 Pauli matrices), which has the common eigenstates of γ_5 for a massless fermion, although the helicity and chirality are completely independent quantities under Lorentz invariance.

In the weak-relativistic regime by expanding the inverse of a mass m (or speed of light c), $\psi_\mu(x)$ is related to an ordinary two-spinor wave function $\psi_s(x)$ ($s = \uparrow, \downarrow$) in the Schrödinger-Pauli equation [47, 48, 49, 50]. The corresponding chiral density in this regime becomes [51, 52, 53]

$$\chi(x) = \sum_{ss'} \psi_s^*(x) \frac{\boldsymbol{\pi} \cdot \boldsymbol{\sigma}_{ss'}}{mc} \psi_{s'}(x), \quad (\boldsymbol{\pi} = \mathbf{p} + \frac{e}{c}\mathbf{A}), \quad (1)$$

where \mathbf{p} , $\boldsymbol{\sigma}$, $-e$, and \mathbf{A} are canonical momentum operator, Pauli matrices, electron charge, and vector potential, respectively, and in the following we consider the case of no external electromagnetic field, $\mathbf{A} = 0$. It should be emphasized that there is no essential distinction between the chirality and helicity in the weak-relativistic regime.

The chiral density operator can be cast into the multipole language in the spherical coordinate by using the mathematical identity [6] for \mathbf{p} in terms of the dimensionless orbital angular-momentum operator $\mathbf{l} = (\mathbf{r} \times \mathbf{p})/\hbar$ as

$$\mathbf{p} = -\frac{\hbar}{r} [\bar{\mathbf{r}} \times \mathbf{l} + i\bar{\mathbf{r}}r \frac{\partial}{\partial r}], \quad \bar{\mathbf{r}} = \frac{\mathbf{r}}{r}, \quad r = |\mathbf{r}|. \quad (2)$$

Then, we obtain the chiral density operator in the multipole language as

$$\hat{\chi} = \frac{\mathbf{p} \cdot \boldsymbol{\sigma}}{mc} = -\frac{\hbar}{mcr} [\bar{\mathbf{r}} \cdot (\mathbf{l} \times \boldsymbol{\sigma}) + i(\bar{\mathbf{r}} \cdot \boldsymbol{\sigma})r \frac{\partial}{\partial r}]. \quad (3)$$

From this expression, we can confirm that $\hat{\chi}$ contains $\hat{G}_0 \propto \bar{\mathbf{r}} \cdot \hat{\mathbf{G}}$ with $\hat{\mathbf{G}} \propto \mathbf{l} \times \boldsymbol{\sigma}$. Moreover, $\hat{\chi}$ also contains $\hat{T}_0 \hat{M}_0$ if the imaginary unit i is regarded as the MT-monopole operator, \hat{T}_0 . Note that $\hat{T}_0 = i$ alone can appear only in the off-diagonal element in more than two-dimensional Hilbert space, as i itself cannot be an hermitian operator. Meanwhile, from Eq. (2), $\bar{\mathbf{r}} \times \mathbf{l}$ is regarded as the MT-dipole type (\mathbf{T}) as \mathbf{p} is categorized to \mathbf{T} as well. In this sense, the relativistic SOC [$\propto (\boldsymbol{\sigma} \times \mathbf{E}) \cdot \mathbf{p}$] is regarded as the coupling between \mathbf{p} (spin-independent MT-dipole operator) and the spin-dependent MT-dipole operator, $\hat{\mathbf{T}} \propto \boldsymbol{\sigma} \times \bar{\mathbf{r}}$ as the dipole moment \mathbf{r} may be proportional to the electric field \mathbf{E} .

For the simplest example of the atomic-scale toroidal multipoles, let us consider the Hilbert space in the total angular momentum $j = 1/2$ ($j_z = \pm 1/2$) arising from s and p orbitals. The

angular dependence of the basis functions in the two-component spinor form are given as

$$\begin{aligned} \psi_{s,+\frac{1}{2}}(\theta, \phi) &= \begin{pmatrix} 1 \\ 0 \end{pmatrix}, & \psi_{s,-\frac{1}{2}}(\theta, \phi) &= \begin{pmatrix} 0 \\ 1 \end{pmatrix}, \\ \psi_{p,+\frac{1}{2}}(\theta, \phi) &= \begin{pmatrix} -\cos\theta \\ -\sin\theta e^{i\phi} \end{pmatrix}, & \psi_{p,-\frac{1}{2}}(\theta, \phi) &= \begin{pmatrix} -\sin\theta e^{-i\phi} \\ \cos\theta \end{pmatrix}. \end{aligned} \quad (4)$$

In this Hilbert space, \hat{G}_0 and \hat{T} apart from the normalization constant are expressed as

$$\hat{G}_0 = \begin{pmatrix} 0 & -i\tilde{\sigma}_0 \\ i\tilde{\sigma}_0 & 0 \end{pmatrix}, \quad \hat{T} = \begin{pmatrix} 0 & -i\tilde{\sigma} \\ i\tilde{\sigma} & 0 \end{pmatrix} \begin{pmatrix} (s) \\ (p) \end{pmatrix}, \quad (5)$$

where $\tilde{\sigma}_0$ and $\tilde{\sigma}$ are the unit and Pauli matrices acting on $j_z = \pm 1/2$ states, while \hat{G} and \hat{T}_0 are inactive in the present Hilbert space.

The eigenstates of \hat{G}_0 are easily obtained as

$$\psi_{a\pm}(\theta, \phi) = \frac{1}{\sqrt{2}} \begin{pmatrix} 1 \mp i \cos\theta \\ \mp i \sin\theta e^{i\phi} \end{pmatrix}, \quad \psi_{b\pm}(\theta, \phi) = \frac{1}{\sqrt{2}} \begin{pmatrix} \mp i \sin\theta e^{-i\phi} \\ 1 \pm i \cos\theta \end{pmatrix}, \quad (6)$$

where the states with the subscript $(a+, b+)$ or $(a-, b-)$ have degenerate eigenvalue of \hat{G}_0 as they are \mathcal{T} partner (\mathcal{T} operation is $-i\tau_y$ and complex conjugation). On the other hand, $(a+, a-)$ or $(b+, b-)$ are \mathcal{P} partner having the eigenvalue of \hat{G}_0 with opposite sign, which is confirmed by applying \mathcal{P} operation, $\theta \rightarrow \pi - \theta$ and $\phi \rightarrow \phi + \pi$. Therefore, such \mathcal{P} partner constitutes a pair of enantiomers of chirality in the atomic scale. The eigenstates of \hat{G}_0 are also those of \hat{T} since \hat{G}_0 and \hat{T} are commutable. In this case, $(a+, b-)$ or $(a-, b+)$ have degenerate eigenvalue of \hat{T}_z as they are \mathcal{TP} partner, while $(a+, a-)$ or $(b+, b-)$ have the eigenvalue of \hat{T}_z with opposite sign.

Although the direct observation for the atomic-scale toroidal multipoles as shown in the above has not been succeeded so far, such microscopic degrees of freedom could be essential ingredients in understanding various cross correlations at microscopic quantum-mechanical level. For clarity of terminology, we use in the following ‘‘atomic’’ multipoles for describing electronic degrees of freedom in terms of orbital and/or spin angular momentum, ‘‘site-cluster’’ multipoles for composite ones consisting of atomic multipoles at several sites in a cluster unit, and ‘‘bond-cluster’’ multipoles for ones on a bond connecting between two sites.

3. Toroidal ordering and related phenomena

In this section, we introduce the relationship between the 32 crystallographic and 122 magnetic point groups and active multipoles with $l = 0, 1$, and the expected cross correlations in the presence of active multipoles.

3.1. Crystallographic point groups and multipoles

The 32 crystallographic point groups (C-PGs) are defined by the group of symmetry operations \mathcal{G} from \mathcal{R} , \mathcal{P} and their combinations, i.e., roto-inversion operation, \mathcal{RP} [$\mathcal{G} \in (\mathcal{R}, \mathcal{P}, \mathcal{RP})$]. Note that the mirror and roto-reflection operations can be expressed by \mathcal{RP} . Since \mathcal{T} is not included in the symmetry operations of C-PG, there is no meaning to distinguish between electric and magnetic properties. Therefore, we discuss the electric multipoles in this subsection by assuming non-magnetic systems.

The relation between C-PGs and active E dipole (\mathbf{Q}) and ET monopole (G_0) and dipole (\mathbf{G}) is shown in Fig. 1 where the number in parenthesis in the Venn diagram indicates that of C-PGs that activates each multipole [12]. The total number of C-PGs for each multipole is listed in Table 1, where Q_0 is always active in 32 C-PGs. Since \mathbf{G} itself does not break the inversion symmetry, the noncentrosymmetric PGs in the \mathbf{G} category (indicated by grey background) should accompany higher-rank odd-parity multipoles. There are 23 C-PGs in Fig. 1, and the rest of nine C-PGs have active multipoles with $l > 1$.

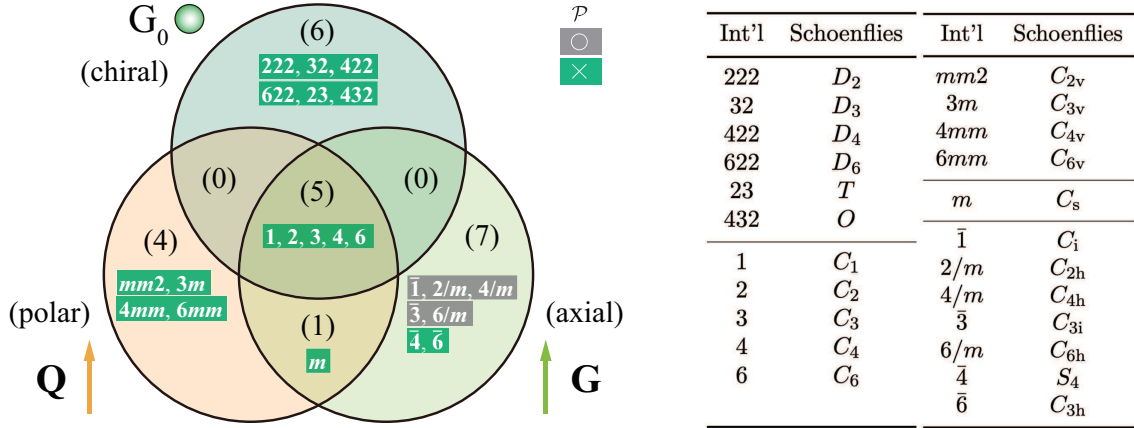


Figure 1. Relation between crystallographic point groups and active electric-type multipoles. The background color of each point group represents the presence or absence of \mathcal{P} symmetry. The additional \mathcal{P} -odd multipoles ($l > 1$) exist in $\bar{4}$ and $\bar{6}$. The correspondence between the international and Schoenflies symbols is also shown.

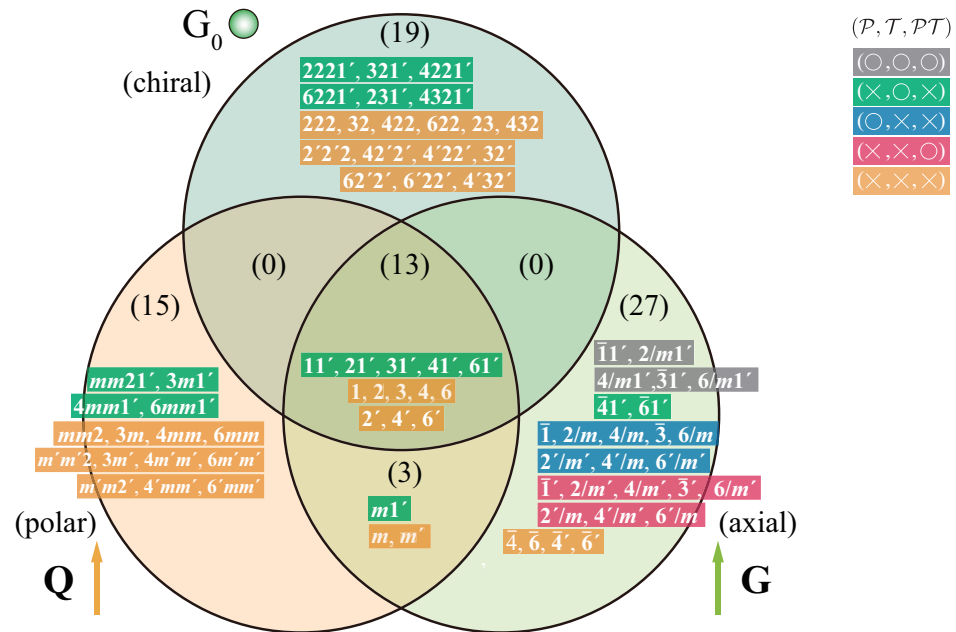
3.2. Magnetic point groups and multipoles

The 122 magnetic point groups (M-PGs) are defined by the combination of \mathcal{T} and symmetry operations of C-PG. They are further classified into three types depending on how \mathcal{T} is included [54]. Type I (32 groups) is the same as C-PGs where \mathcal{T} is completely lost, which is indicated by no operations with prime. Type II (32 groups) called as grey group has the symmetry operations $\mathcal{T}\mathcal{G}$ in addition to \mathcal{G} . This type of M-PG is expressed by attaching $1'$ to the corresponding C-PG. The rest of 58 M-PGs are in Type III called as black-and-white (BW) PG.

Since the presence or absence of \mathcal{T} is taken into account in M-PGs, there is a proper meaning of electric-type and magnetic-type multipoles. The relation between M-PGs and active monopoles and dipoles are shown in Fig. 2 for (a) electric-type multipoles and (b) magnetic-type multipoles, where the number in parenthesis in the Venn diagram indicates that of M-PGs that activates each multipole [55]. The presence or absence of (\mathcal{P} , \mathcal{T} , \mathcal{PT}) is indicated by the background color of each M-PG. There are 77 and 73 M-PGs in Fig. 2(a) and (b), respectively, and the rest of 45 and 49 M-PGs have active electric-type and magnetic-type multipoles with $l > 1$.

The nonmagnetic states accompanying only electric-type multipoles should belong to the Type II grey groups (grey or green backgrounds) which do not appear in Fig. 2(b). For example, 11 chiral states in Type II (green background) are nonmagnetic chiral states, while chiral states such as 222 in Type I and $2'2'2$ in Type III coexist other magnetic-type multipoles, like M_0 and T_0 for 222 and \mathbf{M} and \mathbf{T} for $2'2'2$ as shown in Fig. 2(b). Note that there are symmetry correspondences, T_0M_0 , $\mathbf{T} \cdot \mathbf{M} \leftrightarrow G_0$, indicating that G_0 coexists with \mathbf{T} and \mathbf{M} that are parallel to each other in $2'2'2$. Similarly, 13 axial states in Type II (grey or green backgrounds) are nonmagnetic axial states, while axial states such as $\bar{1}$ in Type I and $\bar{1}'$ in Type III coexist with (M_0, \mathbf{T}) and (T_0, \mathbf{M}) , respectively, as the symmetry correspondence $\mathbf{G} \leftrightarrow T_0\mathbf{M} \leftrightarrow M_0\mathbf{T}$ holds. Moreover, $2'/m$ and $2'/m'$ in Type III coexist \mathbf{T} and \mathbf{M} , respectively, where the symmetry correspondence $\mathbf{G} \leftrightarrow \mathbf{T} \times \mathbf{T}$ or $\mathbf{G} \leftrightarrow \mathbf{M} \times \mathbf{M}$ indicates two distinct vectors $(\mathbf{T}_1, \mathbf{T}_2)$ or $(\mathbf{M}_1, \mathbf{M}_2)$ are orthogonal with each other in $2'/m$ and $2'/m'$, respectively. On the contrary, there is the symmetry correspondences $\mathbf{Q} \leftrightarrow M_0\mathbf{M} \leftrightarrow T_0\mathbf{T}$ and $\mathbf{Q} \leftrightarrow \mathbf{T} \times \mathbf{M}$. Thus, the M-PGs in the intersections of (M_0, \mathbf{M}) and (T_0, \mathbf{T}) in Fig. 2(b) appear in \mathbf{Q} in Fig. 2(a), and \mathbf{T} and \mathbf{M} are orthogonal to each other in $m'm2'$ for example.

(a) Electric-type multipoles



(b) Magnetic-type multipoles

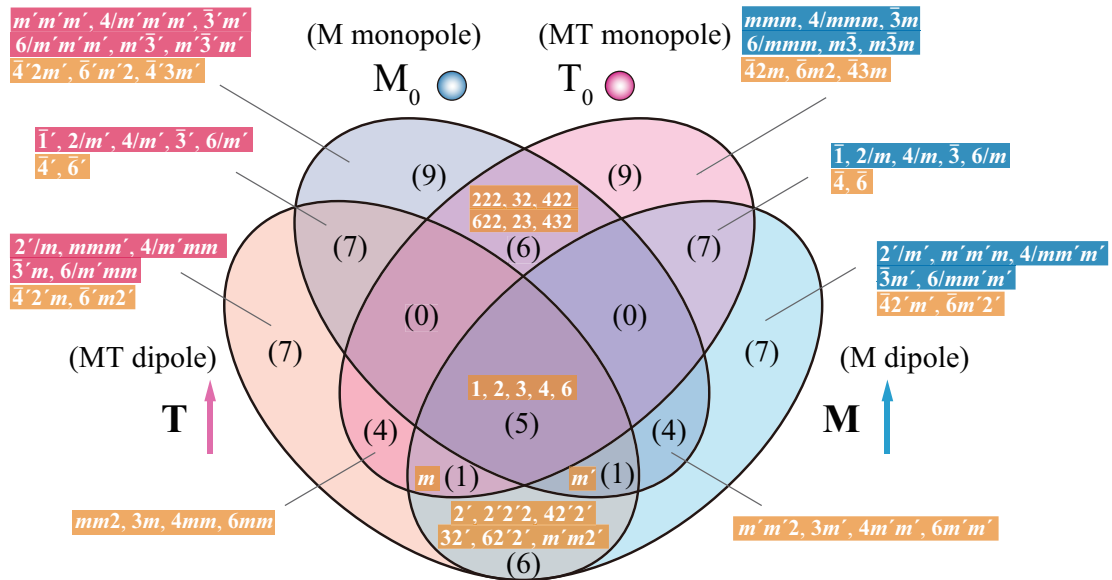


Figure 2. Relation between magnetic point groups and active multipoles. (a) the electric-type multipoles and (b) the magnetic-type multipoles. The background color of each magnetic point group represents the presence or absence of (P, T, PT) symmetries. The additional P -odd multipoles ($l > 1$) exist in the noncentrosymmetric point groups of pure G , T_0 , and M categories.

Table 2. Symmetry correspondences among four-type of multipoles ($l = 0, 1$), conjugated fields, and responses or ordered states.

MP	Conjugate field	Response/Order
Q_0	$\nabla \cdot \mathbf{E}$	δT (temperature difference), charge
M_0	$\mathbf{E} \cdot \mathbf{B}$	monopole-type AFM
G_0	$\mathbf{E} \cdot (\nabla \times \mathbf{E}), \mathbf{B} \cdot (\nabla \times \mathbf{B})$ (optical chirality; Zilch)	chirality
T_0	$\mathbf{E} \cdot (\nabla \times \mathbf{B}), \mathbf{B} \cdot (\nabla \times \mathbf{E})$	MT-monopole-type AFM
\mathbf{Q}	\mathbf{E} (electric field), $-\nabla T$ (temperature gradient)	\mathbf{P} (electric polarization), \mathbf{u} (displacement), ferroelectricity
\mathbf{M}	\mathbf{B} (magnetic field)	\mathbf{M} (magnetization), FM
\mathbf{G}	$\nabla \times \mathbf{E}, \partial \mathbf{B} / \partial t$	$\nabla \times \mathbf{u}$ (static rotational distortion), ferroaxial
\mathbf{T}	$\nabla \times \mathbf{B}, \partial \mathbf{E} / \partial t$	\mathbf{J} (electric current), \mathbf{J}_T (thermal current), vortex-type AFM

It is noted that since (M_0, T_0) or (\mathbf{M}, \mathbf{T}) have opposite properties of $(\mathcal{P}, \mathcal{M}_\perp, \mathcal{M}_\parallel)$, the Venn diagram in Fig. 2(b) becomes symmetric between the left and right sides, where the dual relation, $m \leftrightarrow m'$ and $\bar{n} \leftrightarrow \bar{n}'$ in M-PGs, hold. On the other hand, as the combinations of \mathbf{M} and \mathbf{T} appear differently in \mathbf{G} and \mathbf{Q} , the Venn diagram in Fig. 2(a) becomes asymmetric.

3.3. Cross correlations

As mentioned above, the toroidal multipoles can coexist with other multipoles according to the symmetry correspondence. Even in the high-symmetry PGs such as nonmagnetic grey groups where the equilibrium value of magnetic-type multipoles should vanish, the electric-type multipole can couple with magnetic-type multipoles as a fluctuation. For example, there exists G_0 in $321'$, which can couple with $\mathbf{T} \cdot \mathbf{M}$ as it has the same symmetry properties of G_0 . It also couples with $\mathbf{Q} \cdot \mathbf{G}$ as well. In this case, the Landau free energy can be written as

$$F = \frac{\chi_{\mathbf{T}}^{-1}}{2} \mathbf{T}^2 + \frac{\chi_{\mathbf{M}}^{-1}}{2} \mathbf{M}^2 - \mathbf{M} \cdot \mathbf{H} - \mathbf{T} \cdot (\nabla \times \mathbf{H}) - \alpha G_0 (\mathbf{T} \cdot \mathbf{M}) + \dots, \quad (7)$$

where χ_A is the susceptibility for $A = \mathbf{M}, \mathbf{T}$ and α is the trilinear coupling constant. The third and fourth terms represent the interaction between A and its conjugate field where \mathbf{H} is an external magnetic field. The equilibrium values for \mathbf{M} and \mathbf{T} in the presence of G_0 can be obtained by minimizing F with respect to them as

$$\begin{pmatrix} \mathbf{M} \\ \mathbf{T} \end{pmatrix} = \frac{\chi_{\mathbf{M}} \chi_{\mathbf{T}}}{1 - \chi_{\mathbf{M}} \chi_{\mathbf{T}} (\alpha G_0)^2} \begin{pmatrix} \chi_{\mathbf{T}}^{-1} & \alpha G_0 \\ \alpha G_0 & \chi_{\mathbf{M}}^{-1} \end{pmatrix} \begin{pmatrix} \mathbf{H} \\ \nabla \times \mathbf{H} \end{pmatrix}. \quad (8)$$

From this expression, by applying the electric current, which leads to finite $\nabla \times \mathbf{H}$ along the applied current direction, the magnetic dipole \mathbf{M} is induced linearly through the trilinear coupling. This is nothing but the Edelstein effect, i.e., linear electric-current induced magnetization [56, 57, 58, 59, 60]. It should be noted however that since the situation in the presence of steady current is not an equilibrium state, this type of cross correlation should be treated by the Kubo formula or Boltzmann transport equation, in a rigorous sense [61, 62, 63, 64, 65].

Here, there are a few comments. In the Landau theory, the free energy is constructed under the guidance of symmetry in terms of macroscopic variables irrespective of their microscopic origin. Thus, the argument holds for various microscopic origins of macroscopic variables arising either from cluster-type distributions of classical dipoles or pure quantum-mechanical degrees of freedom. It is often considered the cluster-type toroidal orders where the primary variables are

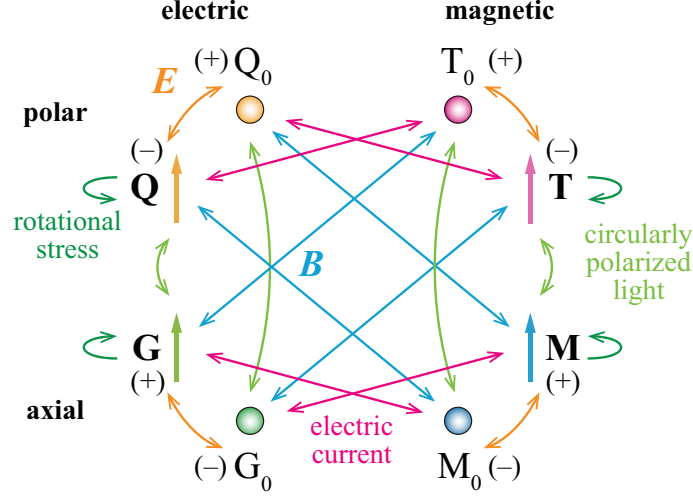


Figure 3. Possible conversion among monopoles and dipoles by external fields: electric field (\mathbf{E}), magnetic field (\mathbf{B}), electric current, rotational stress, and circularly polarized light. The sign in the parenthesis indicates the spatial parity of multipole.

ordinary dipoles. In this case, without using the concept of toroidal moment, the coupling term to a toroidal moment, such as $\mathbf{T} \cdot (\nabla \times \mathbf{H})$ is often dropped. Moreover, a quantum-mechanical type of toroidal order has a finite thermal average of the corresponding toroidal operator itself as discussed in the previous section without any accompanying dipole moments.

In the above discussion, the trilinear term determines possible linear cross correlations. As was already stated, G_0 representing chiral state can couple with $T_0 M_0$, $\mathbf{Q} \cdot \mathbf{G}$, and $\mathbf{T} \cdot \mathbf{M}$. At the same time, the corresponding composite fields of $\mathbf{Q} \cdot \mathbf{G}$ and $\mathbf{T} \cdot \mathbf{M}$, i.e., $\mathbf{E} \cdot (\nabla \times \mathbf{E})$ and $\mathbf{B} \cdot (\nabla \times \mathbf{B})$, whose sum is known as the optical chirality (Zilch) [66, 67, 68] and is activated by circularly polarized light, represent the conjugate field of G_0 [69]. These couplings imply various cross correlations under chiral state, such as the electric-field induced rotational distortion ($\mathbf{E} \rightarrow \mathbf{G}$) [18, 70], the current-induced Magnetization (Edelstein effect) ($\mathbf{J} \rightarrow \mathbf{M}$) [56, 57, 58, 59, 60], and the magnetic-field induced vortex-like spin alignment ($\mathbf{B} \rightarrow \mathbf{T}$).

Similarly, \mathbf{G} representing ferroaxial state can couple with $G_0 \mathbf{Q}$, $T_0 \mathbf{M}$, $M_0 \mathbf{T}$, and $\mathbf{X}_1 \times \mathbf{X}_2$ [71]. These couplings under ferroaxial state lead to the electric-field induced chirality (electrogyration) ($\mathbf{E} \rightarrow G_0$) [5, 35], the magnetic-field induced MT monopole ($\mathbf{B} \rightarrow T_0$), and the transverse responses by fields ($\mathbf{X} \rightarrow \mathbf{G} \times \mathbf{X}$) [17, 72, 73, 74]. The last response will be discussed later.

The MT-monopole T_0 order can be realized in antiferromagnets (AFMs) with proper structures as shown later [23]. In this case, T_0 can couple with $G_0 M_0$, $\mathbf{G} \cdot \mathbf{M}$, and $\mathbf{Q} \cdot \mathbf{T}$. Therefore, we expect the time-reversal switching cross correlations, such as the static electromagnetic-field induced chirality ($\mathbf{E} \cdot \mathbf{B} \rightarrow G_0$), the magnetic-field induced static rotational distortion ($\mathbf{B} \rightarrow \mathbf{G}$), and electric-field induced vortex-like AFM ($\mathbf{E} \rightarrow \mathbf{T}$). The MT-dipole \mathbf{T} orders in some AFMs and the associated cross correlations have already been discussed extensively [2, 3, 26, 75, 76, 77, 78, 79, 80, 81, 82]. \mathbf{T} couples with $\mathbf{G} \cdot \mathbf{T}$, $\mathbf{Q} \cdot \mathbf{M}$ and so on. Among them, the magneto-electric effect ($\mathbf{E} \rightarrow \mathbf{M}$ or $\mathbf{B} \rightarrow \mathbf{Q}$) is the representative cross correlation.

The symmetry correspondence among multipoles ($l = 0, 1$), conjugate fields, and responses or ordered states, and conversion among multipoles by external fields are summarized in Table 2 and Fig. 3. When we consider such analysis for multipoles with $l > 1$, e.g., second-rank stress

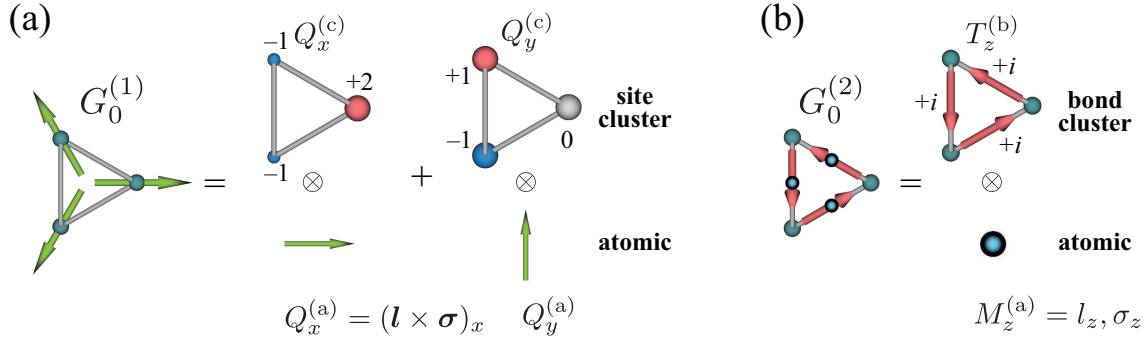


Figure 4. Schematic representations of chirality G_0 , (a) site-cluster type $G_0^{(1)}$ and (b) bond-cluster (itinerant) type $G_0^{(2)}$ [18].

field (Q_{2m}), spin current $J_i M_j$, etc., we expect a further variety of cross correlations with toroidal states in a unified way.

4. Examples

4.1. Chirality as electric-toroidal monopole G_0

As was already mentioned, from a symmetry point of view the definition of chirality matches an ET monopole, G_0 [12, 13, 18, 19]. For example, the typical chiral crystal is elemental tellurium (Te), which belongs to the trigonal space group $P3_121$ ($\#152, D_3^4$) or $P3_221$ ($\#154, D_3^6$) as a pair of right-handed and left-handed enantiomers. In the unit cell, three sublattices constitute the threefold helical chain, representing three-dimensional structural chirality.

The electronic states around H point in the hexagonal Brillouin zone near the Fermi level consist of p orbitals, and they are analyzed by the symmetry-adapted multipole basis [18]. The results show that three types of G_0 give dominant contributions to the tight-binding model of Te,

$$G_0^{(1)} = \frac{1}{\sqrt{2}}(Q_x^{(c)}G_x^{(a)} + Q_y^{(c)}G_y^{(a)}), \quad G_0^{(2)} = T_z^{(b)}M_z^{(a)}, \quad G_0^{(3)} = \frac{1}{\sqrt{2}}(T_x^{(b)}M_x^{(a)} + T_y^{(b)}M_y^{(a)}), \quad (9)$$

where the superscripts, c, b, and a, represent cluster, bond, and atomic bases, respectively, and schematically shown in Fig. 4. Here, $M^{(a)}$ mainly arises from spin degrees of freedom. $G_0^{(1)}$ represents divergent alignment of $\mathbf{G}^{(a)} \propto \mathbf{l} \times \boldsymbol{\sigma}$, while $G_0^{(2)}$ and $G_0^{(3)}$ describe the spin-dependent imaginary hopping processes along and perpendicular to the helical chain, respectively. The latter $G_0^{(2)}$ and $G_0^{(3)}$ are the microscopic origin of Edelstein effect observed by the spectrum shift of ^{125}Te in NMR measurement [58, 60]. On the other hand, $G_0^{(1)}$ can contribute another cross correlation, such as the electro-rotation (electric-field induced rotational distortion) effect ($\mathbf{E} \rightarrow \mathbf{G}$) as discussed in the previous section, since the expression consists of \mathbf{Q} and \mathbf{G} [18]. Once the existence of such microscopic couplings was confirmed by the experiments, one could achieve absolute enantioselection by using composite conjugate fields to access G_0 through such couplings. Note that the ET quadrupole G_u also belongs to the identity representation of D_3 , which gives the monoaxial anisotropy.

There is another attempt to quantify the chirality of molecule by using the ET monopole. For such purpose, a twisted methane is analyzed as a prototype of the method, and the results indeed show that the ET monopole becomes a quantitative indicator for chirality [83]. In the twisted methane, it is clarified that the handedness of chirality corresponds to the sign of the

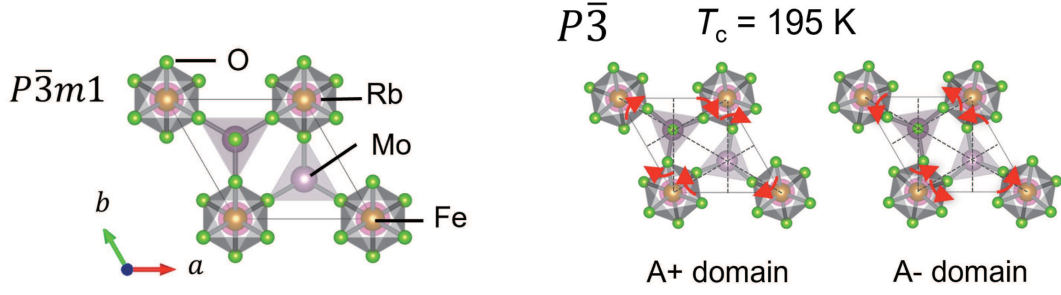


Figure 5. Crystal structure of $\text{RbFe}(\text{MoO}_4)_2$ in (left) normal and (right) ferroaxial phases (modified from [35]). The twin domains appear in the ordered phase depending on the rotated direction of octahedra and tetrahedra units.

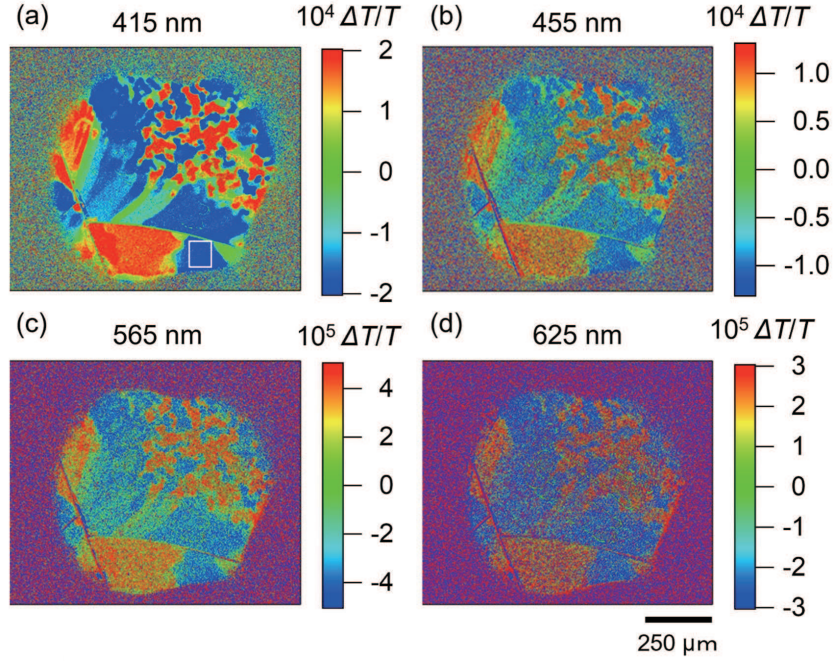


Figure 6. Imaging of the ferroaxial domain structure of $\text{RbFe}(\text{MoO}_4)_2$ by the optical rotation induced by electro-gyration effect, where $\Delta T/T$ is the relative rotation angle of the light polarization [35].

expectation value of the electric toroidal monopole, and that the most important ingredient is the modulation of the spin-dependent imaginary hopping between the hydrogen atoms, while the relativistic spin-orbit coupling within the carbon atom is irrelevant for chirality. The method can be straightforwardly applied to more realistic chiral molecules, which would unveil the nature of chirality quantitatively at the quantum-mechanical level.

4.2. Ferroaxial order (\mathbf{G}), and electro-gyration effect and spin current generation

The ferroaxial order is described by the uniform alignment of \mathbf{G} . $\text{RbFe}(\text{MoO}_4)_2$ is one of the typical crystals showing the ferroaxial order. The crystal structure of this compound is shown in the left panel of Fig. 5, where FeO_6 octahedra sharing vertices with MoO_4 tetrahedra is stacked along c axis. It exhibits the structural phase transition at $T_c \sim 195$ K, in which octahedra and tetrahedra rotate in opposite direction around c axis as shown in the right panel of Fig. 5,

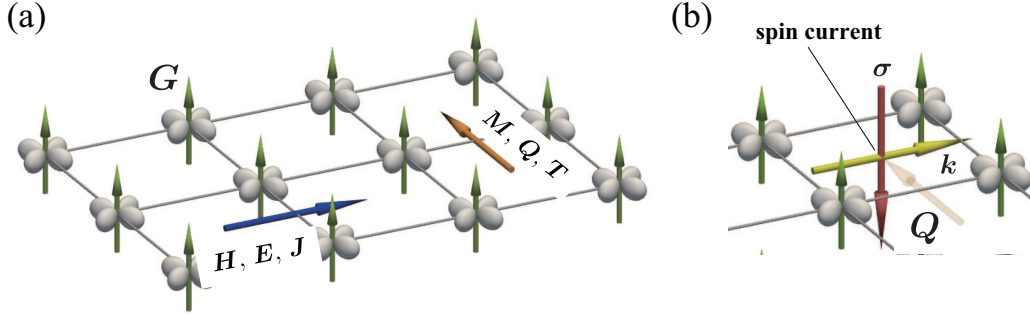


Figure 7. (a) Concept of a nanorotator by \mathbf{G} order. The inputs of \mathbf{H} , \mathbf{E} , and \mathbf{J} can be converted to the transverse output of \mathbf{M} , \mathbf{Q} , and \mathbf{T} , respectively [17]. (b) The electric dipole \mathbf{Q} in the momentum space is equivalent to the spin current perpendicular to \mathbf{Q} .

and the point group changes from $\bar{3}m$ (D_{3d}) to $\bar{3}$ (C_{3i}) with losing vertical mirror operations. This structural transition has been detected by the high-sensitive rotational second-harmonic generation method, in which the electric-quadrupole transition is analyzed [4].

In the ET dipole order \mathbf{G} , the electric field can induce chirality G_0 (electro-gyration effect: $\mathbf{E} \rightarrow G_0$), and the enantioselection, i.e., the sign of G_0 , can be realized by the direction of the electric field as long as the single domain is assumed. In reality, however, there are twin domains, and the electro-gyration effect is utilized for domain detection as shown in Fig. 6 for $\text{RbFe}(\text{MoO}_4)_2$, because the optical rotation angle of the linear polarized light depends on the domain of \mathbf{G} with the fixed applied electric field [35]. The visualization of the ferroaxial domain is particularly important as the achievement of the enantioselection strongly depends on how the domain is distributed in the sample.

A similar method is also applied to NiTiO_3 , which has elucidated that the domain size depends on the cooling rate around T_c [5, 35, 36]. Moreover, state-of-the-art three-dimensional imaging by circularly polarized second harmonic generation microscopy has also been developed to observe the ET dipole in real space [84]. These experimental techniques further stimulate the detection of \mathbf{G} in other candidates, such as $\text{Co}_3\text{Nb}_2\text{O}_8$ [85], $\text{CaMn}_7\text{O}_{12}$ [86], $\text{Ca}_5\text{Ir}_3\text{O}_{12}$ [37, 38, 39, 40, 41], BaCoSiO_4 [87], $\text{K}_2\text{Zr}(\text{PO}_4)_2$ [88], $\text{Na}_2\text{Hf}(\text{BO}_3)_2$ [89], and the typical candidates are $\text{Ca}(\text{BH}_4)_2$ [90], PdS [91], TaPO_5 [92], VPO_5 [93], and NbTe_2 [94] belonging to C_{4h} point group.

In addition to the above conversion from dipole to pseudoscalar, the conversion among dipoles can also be expected in \mathbf{G} order owing to the coupling between \mathbf{G} and $\mathbf{X}_1 \times \mathbf{X}_2$ [17]. This cross correlation is characterized by the conversion where the input and output vectors are orthogonal with each other, and hence \mathbf{G} order plays a role of a nanorotator as shown in Fig. 7(a). Therefore, the inputs of \mathbf{H} , \mathbf{E} , and \mathbf{J} can be converted to the transverse output of \mathbf{M} , \mathbf{Q} , and \mathbf{T} , respectively. In particular, as the electric dipole \mathbf{Q} in the momentum space is expressed as $\mathbf{Q} \propto \mathbf{k} \times \boldsymbol{\sigma}$, the transverse output is equivalent to the longitudinal spin current along the applied electric field as shown in Fig. 7(b). The experimental confirmation of such cross correlation is highly desired.

4.3. Magneto-electric gyration under magnetic-toroidal monopole order (T_0)

As discussed in the previous section, a divergent alignment of the vortex-like AFM represents the cluster-type MT monopole, T_0 [23]. Indeed, AFMs belonging to the same paramagnetic point group only without \mathcal{T} operation, i.e., Type I magnetic point group, can exhibit the MT monopole order, and they accompany additional multipoles in low-symmetry point groups. The classification of active multipoles and the candidate AFMs are summarized in Table 3.

Table 3. Classification for magnetic-toroidal monopole order (T_0) in Type I magnetic point groups and candidate materials [23]. Other multipoles indicated by open circles are accompanied with T_0 order.

PG	T_0	M_z	T_z	M_0	Materials
$O_h, T_d, T_h, D_{2h}, D_{3h}, D_{4h}, D_{6h}, D_{2d}, D_{3d}$	○				KMnF ₃ , Ca ₂ RuO ₄
$C_{2h}, C_{3h}, C_{4h}, C_{6h}, S_4, C_{3i}, C_i$	○	○			MnV ₂ O ₄ , Mn ₃ As ₂
$C_{2v}, C_{3v}, C_{4v}, C_{6v}$	○		○		YMnO ₃ , Er ₂ Cu ₂ O ₅
O, T, D_2, D_3, D_4, D_6	○			○	Ho ₂ Ge ₂ O ₇ , Mn ₃ IrGe
C_s	○	○	○		Mn ₄ Nb ₂ O ₉
C_1, C_2, C_3, C_4, C_6	○	○	○	○	ScMnO ₃ , Mn ₂ FeMoO ₆

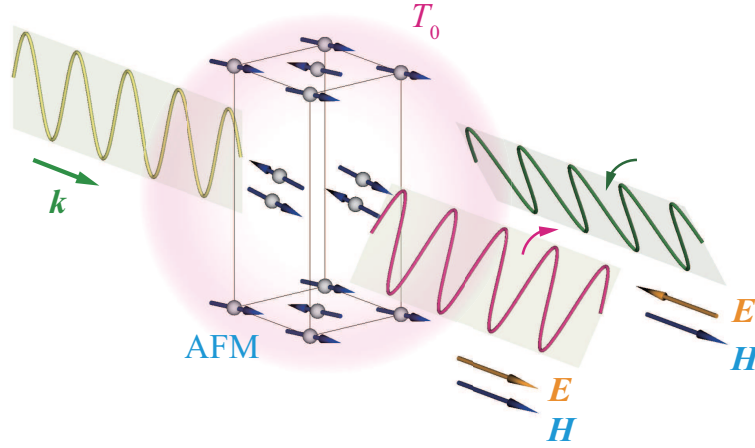


Figure 8. Magnetic structure in Ca₂RuO₄ accompanying T_0 , and expected optical rotation measurement in the applied electric and magnetic fields, \mathbf{E} and \mathbf{H} [23]. The rotation angle depends on the parallel or anti-parallel fields of \mathbf{E} and \mathbf{H} .

Table 4. Magnetic moments at four Ru sites in Ca₂RuO₄ [95]. $\mathbf{T}_u^{(c)}$, $\mathbf{T}_v^{(c)}$, and $\mathbf{M}_{xyz}^{(c)}$ represent the cluster $3z^2 - r^2$ -type and $x^2 - y^2$ -type MT quadrupoles, and xyz -type magnetic octupole, respectively, which are all belonging to the identity representation.

Position	\mathbf{M}	$\mathbf{T}_u^{(c)}$	$\mathbf{T}_v^{(c)}$	$\mathbf{M}_{xyz}^{(c)}$
(0, 0, 0)	(0, +1.0, +0.1)	$\frac{1}{2\sqrt{2}}(1, -1, 0)$	$\frac{1}{2\sqrt{6}}(1, 1, -2)$	$\frac{1}{2\sqrt{3}}(1, 1, 1)$
(1/2, 0, 1/2)	(0, -1.0, -0.1)	$\frac{1}{2\sqrt{2}}(-1, 1, 0)$	$\frac{1}{2\sqrt{6}}(-1, -1, -2)$	$\frac{1}{2\sqrt{3}}(-1, -1, 1)$
(0, 1/2, 1/2)	(0, +1.0, -0.1)	$\frac{1}{2\sqrt{2}}(-1, -1, 0)$	$\frac{1}{2\sqrt{6}}(-1, 1, 2)$	$\frac{1}{2\sqrt{3}}(-1, 1, -1)$
(1/2, 1/2, 0)	(0, -1.0, -0.1)	$\frac{1}{2\sqrt{2}}(1, 1, 0)$	$\frac{1}{2\sqrt{6}}(1, -1, 2)$	$\frac{1}{2\sqrt{3}}(1, -1, -1)$

Among them, Ca₂RuO₄ for example shows AFM order ($mmm1' \rightarrow mmm, D_{2h}$) as shown in Fig. 8, and the ordered moment at each position is given by \mathbf{M} in Table 4. There are nine cluster-type magnetic multipoles, $\mathbf{T}_u^{(c)}$, $\mathbf{T}_v^{(c)}$, and $\mathbf{M}_{xyz}^{(c)}$, belonging to the identity representation,

and the observed magnetic structure can be expressed as the linear combination as

$$\mathbf{M} = -1.414\mathbf{T}_u^{(c)} + 0.653\mathbf{T}_v^{(c)} + 1.270\mathbf{M}_{xyz}^{(c)}. \quad (10)$$

Therefore, we expect various cross correlations in the presence of T_0 as discussed previously. For example, a possible experimental setup is shown in Fig. 8, which is expected to show the optical rotation in the presence of static electric and magnetic fields, and the rotation angle depends on the relative directions between electric and magnetic fields. The direction of incident light can be chosen arbitrarily since the order parameter has a scalar nature. In this experiment, it would be also important to know how the domain of T_0 is distributed in the sample. This type of experiment also provides a way of absolute enantioselection by static electric and magnetic fields as long as the single domain is assumed.

5. Summary

In summary, we have introduced the concept of toroidal multipoles both from classical and quantum viewpoint. By using the concept, we have shown the correspondence between active multipoles and crystallographic point groups in non-magnetic materials, and magnetic point groups in magnetic materials, with focusing on monopoles and dipoles. The electric-toroidal monopole is a practical entity of chirality, while the electric-toroidal dipole is a microscopic variable of ferroaxial order. The magnetic-toroidal monopole and dipole are often realized in certain type of antiferromagnets. Once the relevant symmetry-adapted multipoles are identified in materials, we can expect various cross correlations in a unified way at the quantum-mechanical level. The proper understanding of these toroidal moments would stimulate further investigation of mutual conversions among peculiar states of matter.

Acknowledgement

This paper is based on fruitful collaborations with Yuki Yanagi, Megumi Yatsushiro, Rikuto Oiwa, Jun-ichiro Kishine, and Hiroshi H. Yamamoto. We would also like to thank Makoto Naka, Michi-to Suzuki, Yukitoshi Motome, Hitoshi Seo, Takuya Nomoto, Ryotaro Arita, Hiroshi Amitsuka, Tatsuya Yanagisawa, Takahisa Arima, Hiraku Saito, for helpful discussions. This research was supported by JSPS KAKENHI Grants Numbers JP21H01031, JP21H01037, JP22H04468, JP22H00101, JP22H01183, JP23K03288, JP23H04869, JP23H00091 and by JST PRESTO (JP- MJPR20L8) and JST CREST (JPMJCR23O4), and the grants of Special Project (IMS program 23IMS1101), and OML Project (NINS program No. OML012301) by the National Institutes of Natural Sciences.

- [1] Van Aken B B, Rivera J P, Schmid H and Fiebig M 2007 *Nature* **449** 702–705
- [2] Spaldin N A, Fiebig M and Mostovoy M 2008 *J. Phys.: Condens. Matter* **20** 434203
- [3] Kopaev Y V 2009 *Physics-Uspekhi* **52** 1111–1125
- [4] Jin W, Druke E, Li S, Admasu A, Owen R, Day M, Sun K, Cheong S W and Zhao L 2020 *Nat. Phys.* **16** 42–46
- [5] Hayashida T, Uemura Y, Kimura K, Matsuoka S, Morikawa D, Hirose S, Tsuda K, Hasegawa T and Kimura T 2020 *Nat. Commun.* **11** 4582
- [6] Kusunose H 2008 *J. Phys. Soc. Jpn.* **77** 064710
- [7] Kuramoto Y, Kusunose H and Kiss A 2009 *J. Phys. Soc. Jpn.* **78** 072001
- [8] Santini P, Carretta S, Amoretti G, Caciuffo R, Magnani N and Lander G H 2009 *Rev. Mod. Phys.* **81**(2) 807–863
- [9] Dubovik V, Tosunyan L and Tugushev V 1986 *Zh. Eksp. Teor. Fiz* **90** 590
- [10] Dubovik V and Tugushev V 1990 *Phys. Rep.* **187** 145–202
- [11] Hayami S and Kusunose H 2018 *J. Phys. Soc. Jpn.* **87** 033709
- [12] Hayami S, Yatsushiro M, Yanagi Y and Kusunose H 2018 *Phys. Rev. B* **98**(16) 165110
- [13] Kusunose H, Oiwa R and Hayami S 2020 *J. Phys. Soc. Jpn.* **89** 104704
- [14] Kusunose H and Hayami S 2022 *J. Phys.: Condens. Matter* **34** 464002

- [15] Hayami S and Kusunose H 2024 *under review*
- [16] Kusunose H, Oiwa R and Hayami S 2023 *Phys. Rev. B* **107**(19) 195118
- [17] Hayami S, Oiwa R and Kusunose H 2022 *J. Phys. Soc. Jpn.* **91** 113702
- [18] Oiwa R and Kusunose H 2022 *Phys. Rev. Lett.* **129**(11) 116401
- [19] Kishine J i, Kusunose H and Yamamoto H M 2022 *Isr. J. Chem.* **62** e202200049
- [20] Barron L 1986 *Chem. Soc. Rev.* **15** 189–223
- [21] Barron L D 1986 *J. Am. Chem. Soc.* **108** 5539–5542
- [22] Barron L D 2004 *Molecular Light Scattering and Optical Activity* 2nd ed (Cambridge University Press)
- [23] Hayami S and Kusunose H 2023 *Phys. Rev. B* **108**(14) L140409
- [24] Saito H, Uenishi K, Miura N, Tabata C, Hidaka H, Yanagisawa T and Amitsuka H 2018 *J. Phys. Soc. Jpn.* **87** 033702
- [25] Ota K, Shimozawa M, Muroya T, Miyamoto T, Hosoi S, Nakamura A, Homma Y, Honda F, Aoki D and Izawa K 2022 *arXiv:2205.05555*
- [26] Hayami S, Kusunose H and Motome Y 2014 *Phys. Rev. B* **90**(2) 024432
- [27] Ishitobi T and Hattori K 2023 *Phys. Rev. B* **107**(10) 104413
- [28] Gitgeatpong G, Zhao Y, Avdeev M, Piltz R O, Sato T J and Matan K 2015 *Phys. Rev. B* **92**(2) 024423
- [29] Gitgeatpong G, Suewattana M, Zhang S, Miyake A, Tokunaga M, Chanlert P, Kurita N, Tanaka H, Sato T J, Zhao Y and Matan K 2017 *Phys. Rev. B* **95**(24) 245119
- [30] Gitgeatpong G, Zhao Y, Piyawongwatthana P, Qiu Y, Harriger L W, Butch N P, Sato T J and Matan K 2017 *Phys. Rev. Lett.* **119**(4) 047201
- [31] Hayami S, Kusunose H and Motome Y 2016 *J. Phys. Soc. Jpn.* **85** 053705
- [32] Wadley P, Novák V, Champion R, Rinaldi C, Martí X, Reichlová H, Železný J, Gazquez J, Roldan M, Varela M *et al.* 2013 *Nat. Commun.* **4** 2322
- [33] Wadley P, Howells B, Železný J, Andrews C, Hills V, Champion R P, Novák V, Olejník K, Maccherozzi F, Dhési S *et al.* 2016 *Science* **351** 587–590
- [34] Wang C, Gao Y and Xiao D 2021 *Phys. Rev. Lett.* **127**(27) 277201
- [35] Hayashida T, Uemura Y, Kimura K, Matsuoka S, Hagihala M, Hirose S, Morioka H, Hasegawa T and Kimura T 2021 *Phys. Rev. Materials* **5**(12) 124409
- [36] Fang X, De C, Huang F T, Xu X, Du K, Wang K, Li B and Cheong S W 2023 *J. Am. Chem. Soc.* **145** 28022–28029
- [37] Hasegawa T, Yoshida W, Nakamura K, Ogita N and Matsuhira K 2020 *J. Phys. Soc. Jpn.* **89** 054602
- [38] Hanate H, Hasegawa T, Tsutsui S, Nakamura K, Yoshimoto Y, Kishigami N, Haneta S and Matsuhira K 2020 *J. Phys. Soc. Jpn.* **89** 053601
- [39] Hanate H, Hasegawa T, Hayami S, Tsutsui S, Kawano S and Matsuhira K 2021 *J. Phys. Soc. Jpn.* **90** 063702
- [40] Hayami S, Tsutsui S, Hanate H, Nagasawa N, Yoda Y and Matsuhira K 2023 *J. Phys. Soc. Jpn.* **92** 033702
- [41] Hanate H, Tsutsui S, Yajima T, Nakao H, Sagayama H, Hasegawa T and Matsuhira K 2023 *J. Phys. Soc. Jpn.* **92** 063601
- [42] Kelvin W T B 1894 *The molecular tactics of a crystal* (Clarendon Press)
- [43] Kelvin W T B 2010 *Baltimore lectures on molecular dynamics and the wave theory of light* (Cambridge University Press)
- [44] Sakurai J J 1967 *Advanced Quantum Mechanics* (Addison-Wesley, Massachusetts)
- [45] Baym G 1969 *Lectures on Quantum Mechanics* (Westview Press, Colorado)
- [46] Peskin M E and Schroeder D V 1995 *An Introduction to Quantum Field Theory* (Westview Press, Colorado)
- [47] Foldy L L and Wouthuysen S A 1950 *Phys. Rev.* **78**(1) 29–36
- [48] Gurtler R and Hestenes D 1975 *J. Math. Phys.* **16** 573–584
- [49] Wang Y, Xia K, Su Z B and Ma Z 2006 *Phys. Rev. Lett.* **96**(6) 066601
- [50] Chen T W and Chiou D W 2014 *Phys. Rev. A* **90**(1) 012112
- [51] Banerjee R and Chatterjee D 2020 *Nucl. Phys. B* **954** 114994
- [52] Abanov A G and Wiegmann P B 2022 *Phys. Rev. Lett.* **128**(5) 054501
- [53] Hoshino S, Suzuki M T and Ikeda H 2023 *Phys. Rev. Lett.* **130**(25) 256801
- [54] Bradley C and Cracknell A 2009 *The mathematical theory of symmetry in solids: representation theory for point groups and space groups* (Oxford University Press)
- [55] Yatsushiro M, Kusunose H and Hayami S 2021 *Phys. Rev. B* **104**(5) 054412
- [56] Edelstein V M 1990 *Solid State Commun.* **73** 233–235
- [57] Yoda T, Yokoyama T and Murakami S 2015 *Sci. Rep.* **5** 12024
- [58] Furukawa T, Shimokawa Y, Kobayashi K and Itou T 2017 *Nat. Commun.* **8** 954
- [59] Yoda T, Yokoyama T and Murakami S 2018 *Nano Lett.* **18** 916–920
- [60] Furukawa T, Watanabe Y, Ogasawara N, Kobayashi K and Itou T 2021 *Phys. Rev. Res.* **3**(2) 023111
- [61] Sodemann I and Fu L 2015 *Phys. Rev. Lett.* **115**(21) 216806

- [62] Gao Y, Zhang Y and Xiao D 2020 *Phys. Rev. Lett.* **124**(7) 077401
- [63] Watanabe H and Yanase Y 2020 *Phys. Rev. Research* **2**(4) 043081
- [64] Watanabe H and Yanase Y 2021 *Phys. Rev. X* **11**(1) 011001
- [65] Oiwa R and Kusunose H 2022 *J. Phys. Soc. Jpn.* **91** 014701
- [66] Lipkin D M 1964 *J. Math. Phys.* **5** 696–700
- [67] Kibble T 1965 *J. Math. Phys.* **6** 1022–1026
- [68] Proskurin I, Ovchinnikov A S, Nosov P and Kishine J i 2017 *New J. Phys.* **19** 063021
- [69] Hayami S, Yambe R and Kusunose H 2023 *arXiv:2312.07735*
- [70] Hayami S and Kusunose H 2023 *J. Phys. Soc. Jpn.* **92** 113704
- [71] Hayami S 2022 *Phys. Rev. B* **106**(14) 144402
- [72] Nasu J and Hayami S 2022 *Phys. Rev. B* **105**(24) 245125
- [73] Inda A and Hayami S 2023 *J. Phys. Soc. Jpn.* **92** 043701
- [74] Kirikoshi A and Hayami S 2023 *J. Phys. Soc. Jpn.* **92** 123703
- [75] Fiebig M 2005 *J. Phys. D: Appl. Phys.* **38** R123
- [76] Khomskii D 2009 *Physics* **2** 20
- [77] Hayami S, Kusunose H and Motome Y 2016 *J. Phys.: Condens. Matter* **28** 395601
- [78] Gao Y and Xiao D 2018 *Phys. Rev. B* **98**(6) 060402(R)
- [79] Shitade A, Watanabe H and Yanase Y 2018 *Phys. Rev. B* **98**(2) 020407(R)
- [80] Yatsushiro M, Oiwa R, Kusunose H and Hayami S 2022 *Phys. Rev. B* **105**(15) 155157
- [81] Hayami S, Yatsushiro M and Kusunose H 2022 *Phys. Rev. B* **106**(2) 024405
- [82] Kirikoshi A and Hayami S 2023 *Phys. Rev. B* **107**(15) 155109
- [83] Inda A, Oiwa R, Hayami S, Yamamoto H M and Kusunose H 2024 *arXiv:2402.13611*
- [84] Yokota H, Hayashida T, Kitahara D and Kimura T 2022 *npj Quantum Mater.* **7** 106
- [85] Johnson R D, Nair S, Chapon L C, Bombardi A, Vecchini C, Prabhakaran D, Boothroyd A T and Radaelli P G 2011 *Phys. Rev. Lett.* **107**(13) 137205
- [86] Johnson R D, Chapon L C, Khalyavin D D, Manuel P, Radaelli P G and Martin C 2012 *Phys. Rev. Lett.* **108**(6) 067201
- [87] Xu X, Huang F T, Admasu A S, Kratochvílová M, Chu M W, Park J G and Cheong S W 2022 *Phys. Rev. B* **105**(18) 184407
- [88] Yamagishi S, Hayashida T, Misawa R, Kimura K, Hagihala M, Murata T, Hirose S and Kimura T 2023 *Chem. Mater.* **35** 747–754
- [89] Nagai T and Kimura T 2023 *Chem. Mater.* **35** 4109–4115
- [90] Filinchuk Y, Rönnebro E and Chandra D 2009 *Acta Mater.* **57** 732–738
- [91] Brese N E, Squattrito P J and Ibers J A 1985 *Acta Crystallogr.* **41** 1829–1830
- [92] Longo J, Pierce J and Kafalas J 1971 *Mate. Res. Bull.* **6** 1157–1165
- [93] Gautier R, Gautier R, Hernandez O, Audebrand N, Bataille T, Roiland C, Elkaïm E, Le Pollès L, Furet E and Le Fur E 2013 *Dalton Trans.* **42** 8124–8131
- [94] Bhatt N, Vaidya R, Patel S and Jani A 2004 *Bull. Mater. Sci.* **27** 23–25
- [95] Porter D G, Granata V, Forte F, Di Matteo S, Cuoco M, Fittipaldi R, Vecchione A and Bombardi A 2018 *Phys. Rev. B* **98**(12) 125142